High-Dimensional Quantum Cryptography with Hybrid Orbital-Angular-Momentum States through 25 km of Ring-Core Fiber: A Proof-of-Concept Demonstration

Qian-Ke Wang,[1] Fang-Xiang Wang,[2,3,*] Jun Liu,[1] Wei Chen,[2,3] Zheng-Fu Han,[2,3] Andrew Forbes,[1,4] and Jian Wang[1,†]

[1] *Wuhan National Laboratory for Optoelectronics and School of Optical and Electronic Information, Huazhong University of Science and Technology, Wuhan, 430074 Hubei, China*

[2] *CAS Key Laboratory of Quantum Information, University of Science and Technology of China, Hefei, 230026 Anhui, China*

[3] *CAS Center for Excellence in Quantum Information and Quantum Physics, University of Science and Technology of China, Hefei, 230026 Anhui, China*

[4] *School of Physics, University of the Witwatersrand, Private Bag, 3, Wits, Johannesburg, 2050, South Africa*

(Received 1 March 2021; revised 7 May 2021; accepted 27 May 2021; published 14 June 2021)

Quantum cryptography provides the inherent security for transmitting confidential information across free space or a fiber link. However, a high secure-key rate is still a challenge for a quantum-cryptography system. High-dimensional quantum cryptography, which can tolerate much higher channel noise, is a prospective way to share a higher secure-key rate between legitimate users, and has received substantial attention over the last decade. In particular, orbital angular momentum (OAM) can provide an abundant resource for high-dimensional quantum cryptography. Furthermore, combining spin angular momentum (SAM) with OAM can increase the encoding alphabet. Here we verify a prepare-and-measure quantum-cryptography scheme based on four-dimensional SAM-OAM hybrid states over kilometer-scale ring-core fibers. The measured quantum-bit error rates are 4.3% for 4 km of fiber and 16.3% for 25 km of fiber. The scheme simplifies the process of state preparation and measurement, with a compact and scalable setup.

DOI: 10.1103/PhysRevApplied.15.064034

I. INTRODUCTION

Quantum cryptography offers a reliable way to secure the communication of sensitive information, which is guaranteed by physical laws [1,2]. By performing specific protocols, one can determine whether there has been eavesdropping of messages. Utilizing a higher-order Hilbert space not only increases the secret-key rate but also makes legitimate users more capable of detecting eavesdroppers [3]. Moreover, noise tolerance would be improved with the increase of dimensions [4–6]. We can take advantage of this fact when implementing high-dimensional quantum-cryptography schemes over noisy links.

Among all photon degrees of freedom, orbital angular momentum (OAM) of the photon is a promising high-dimensional resource owing to the inherent infinite number of topological charge values [7], which are orthogonal to each other, the ease of measurement, and the fact that they form a natural Schmidt basis. Photons with more than 10 000-order topological charges of OAM have been realized in the laboratory, leaving tremendous space for exploration experimentally [8]. Polarization, also known as spin angular momentum (SAM), is another photon degree of freedom, and has been well investigated in both the classical communication realm and the quantum communication realm. Photons with structured intensity, polarization, and phase are recognized as structured photons [9], among which SAM-OAM hybrid states are the most commonly used. Although progress in harnessing high-dimensional spatial mode entanglement remains in its infancy [10], there has been much effort to transmit quantum SAM-OAM hybrid entanglement states through various media (e.g., free space [11–13], water [14], and fiber [15,16]) in different application scenarios.

The nonseparable nature of OAM and SAM makes them interchangeable [17,18], and thus the preparation and measurement process of quantum key distribution (QKD) based on SAM-OAM hybrid states could be simplified. In the manner of prepare-and-measure QKD, researchers have achieved free-space high-dimensional quantum key distribution (HDQKD) by this principle [19]. To bring quantum networks to fruition, transmitting high-dimensional hybrid states over a kilometer-scale distance, fibers that support hybrid states are crucial. Achieving

*fxwung@ustc.edu.cn
†jwang@hust.edu.cn

mode stability in a fiber requires separation of the propagation constants β, and according to Ref. [20] a waveguide whose profile mirrors that of the mode itself would be more suitable for maximizing differential propagation constants $\delta\beta$. The index profile of ring-core fiber (RCF) is compatible with the donut-shaped OAM fields, which is beneficial to suppress the unwanted radial higher-order modes. This simplifies the multiplexing and demultiplexing of the OAM modes, and prevents crossing between effective indices of modes from different mode groups, allowing good mode separation. In addition, in comparison with a mode-division multiplexing system using multimode fibers, fiber-optic OAM multiplexing communications using RCFs can simplify or even avoid the complex multiple-input and multiple-output digital signal processing traditionally used to mitigate the mode crosstalk. In the last decade, optimized design of RCFs has led to a significant increase in the number of OAM modes and the length of RCFs in fiber-optic OAM multiplexing communication systems [21–24]. There are also several other specially designed fibers that support transmission of OAM modes, including circular photonic crystal fiber [25], inverse-parabolic graded-index fiber [26], supermode fiber [27], and air-core fiber [28,29]. The use of structured photons to implement QKD in a 60-m vortex fiber has been demonstrated [15]. Recently, high-dimensional OAM-entanglement distribution over 1 km of few-mode fiber [30] and a real-time HDQKD test through a 1.2-km air-core fiber with negligible mode mixing between the OAM modes were achieved [16]. These experiments increase the distribution of high-dimensional quantum states, attesting OAM as a resource for the future quantum network. However, a major limitation of this approach is the accessibility of air-core fiber.

In this paper, we demonstrate a proof-of-concept high-dimensional quantum-cryptography scheme to encode and transmit SAM-OAM hybrid states through 4- and 25-km RCFs, which are relatively easy to acquire. We realize it by preparing and projectively measuring two sets of mutually unbiased bases (MUBs) in a four-dimensional Hilbert space. Mode indistinguishability in time and orthogonality are conserved throughout the fiber. We test the output states with two kinds of measuring apparatus. The probability distribution of the projective measurement after the fiber is characterized and yields a quantum-bit error rate (QBER) of up to 4.3% for 4 km of fiber and 16.3% for 25 km of fiber. Our work is a useful advance in the aspects of information per photon and state-distribution distance, revealing the feasibility of HDQKD over conventional RCFs.

II. CONCEPT AND PRINCIPLE

The concept of transmission of high-dimensional quantum states in fiber is illustrated in Fig. 1. The input linearly polarized Gaussian beam is converted into a different mode distribution after the spin-orbit-coupling, OAM-mapping, and SAM-mapping processes. The product of SAM and OAM superposition states forms the so-called SAM-OAM hybrid state basis, which fully exploits the photon degrees of freedom and fiber transmission characteristics. After transmission through the kilometer-scale RCF, the projective-measurement operations are performed by another three major processes: SAM measurement, spin-orbit coupling, and OAM measurement. Afterward, the detected mode intensity after transmission may indicate which mode is incoming and its fidelity. All the apparatus for the three major processes are not constrained by what is illustrated in Fig. 1. An apparatus might be able to perform both spin-orbit coupling and OAM measurement [e.g., a spatial light modulator (SLM)]. The details of the setup are given in Sec. III.

The nonseparable SAM-OAM hybrid states are so-called vector vortices [31]. The vector-vortex states are the superposition of OAM modes. Those states on the equator of the high-order Poincaré sphere [32] are given by

$$|S\rangle = \frac{1}{\sqrt{2}}\left(|L\rangle|-\ell\rangle + e^{i\theta}|R\rangle|\ell\rangle\right), \tag{1}$$

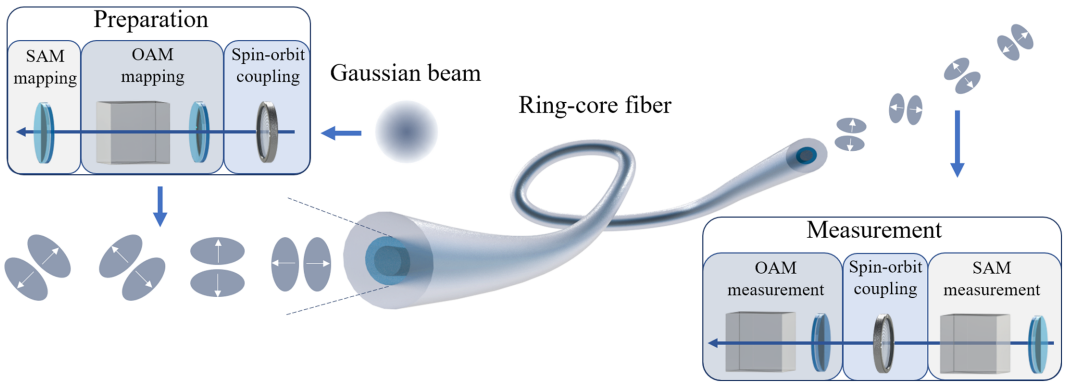

FIG. 1. Concept of transmission of high-dimensional quantum states in RCF.

where $|L\rangle$ and $|R\rangle$ are the left and right circular polarization in the form of Dirac notation, respectively, and $|\pm\ell\rangle$ stands for OAM modes with topological charge $\pm\ell$. The key to prepare and measure these states lies in the spin-orbit coupling; namely, an interaction between SAM and OAM. There are several approaches to achieving this; for instance, by metasurfaces [33] or q plates [18,19,34,35], which we use in this study. A q plate with no phase retardation has its operator defined by

$$\hat{Q}(q) = (|L\rangle\langle R|) \otimes \left(\sum_{\ell} |\ell - 2q\rangle\langle\ell|\right) + (|R\rangle\langle L|) \otimes \left(\sum_{\ell} |\ell + 2q\rangle\langle\ell|\right), \quad (2)$$

where q is the charge of the q plate [36,37]. For a horizontally polarized Gaussian beam $|H\rangle|0\rangle$, the output state after a q plate is

$$|O_H\rangle = \hat{Q}(q)|H\rangle|0\rangle = (|R\rangle|2q\rangle + |L\rangle|-2q\rangle)/\sqrt{2}, \quad (3)$$

which is a radially polarized vector-vortex state and in the form of Eq. (1). A vertically polarized Gaussian beam follows the same rule but yields an azimuthally polarized vector vortex.

When projected into arbitrary linear polarization with projection angle α_1

$$\hat{P}_S(\alpha_1) = (\cos\alpha_1|H\rangle + \sin\alpha_1|V\rangle)(\cos\alpha_1\langle H| + \sin\alpha_1\langle V|), \quad (4)$$

the state transforms into

$$\hat{P}_S(\alpha_1)|O_H\rangle = \frac{e^{-i\alpha_1}}{2}(\cos\alpha_1|H\rangle + \sin\alpha_1|V\rangle) \times \left(|2q\rangle + e^{2i\alpha_1}|-2q\rangle\right). \quad (5)$$

The projective state becomes a product state of polarization and OAM with a factor α_1 in both fractions. Hence, adjusting the projective angle α_1 gives the ability to manipulate both SAM and OAM of the photon simultaneously. This operation, which is the central principle of state generation in Fig. 2, simplifies the process of preparing and measuring SAM-OAM hybrid states. To structure two sets of four-dimensional MUBs, two independent variables are needed. By application of a unitary transformation of polarization $\hat{U}_S(\alpha_2)$ to Eq. (5), it transforms into

$$\hat{U}_S(\alpha_2)\hat{P}_S(\alpha_1)|O_H\rangle = \frac{e^{-i\alpha_1}}{2}[\cos(\alpha_2 - \alpha_1)|H\rangle + \sin(\alpha_2 - \alpha_1)|V\rangle] \times \left(|2q\rangle + e^{2i\alpha_1}|-2q\rangle\right), \quad (6)$$

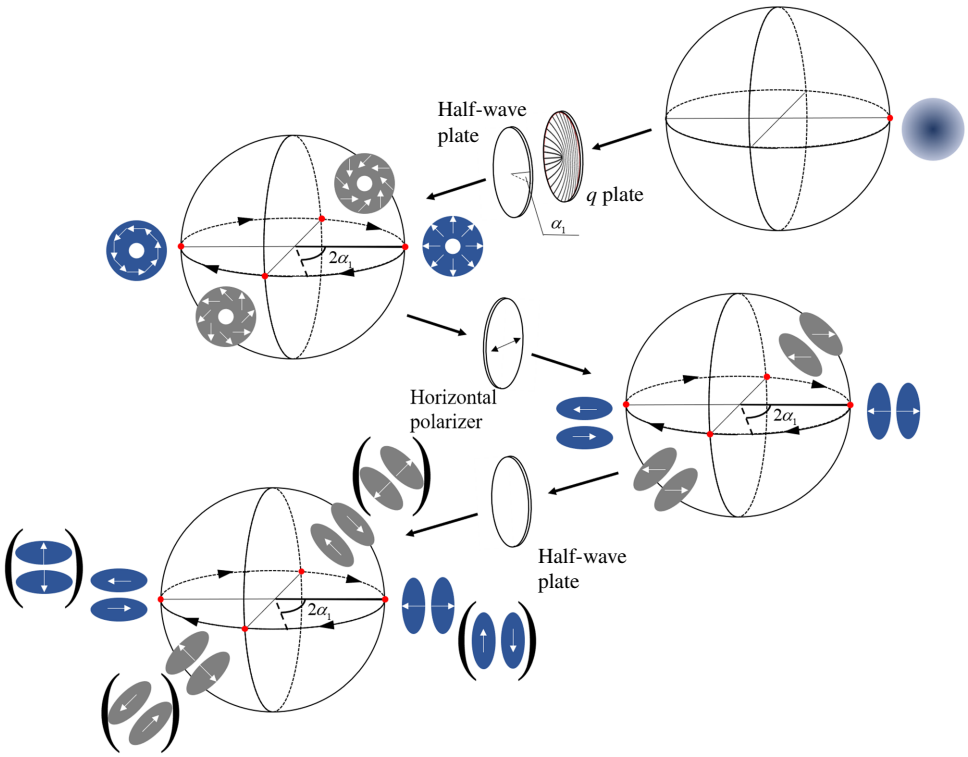

FIG. 2. Principle of state preparation. The Poincaré sphere presents the transformation of the states.

TABLE I. Generation of two groups of MUBs at the input.

State	$\hat{U}_S(\alpha_1)$	$\hat{U}_S(\alpha_2)$	State	$\hat{U}_S(\alpha_1)$	$\hat{U}_S(\alpha_2)$
$\|\psi_1\rangle(\|\xi_1\rangle)$	0	0	$\|\phi_1\rangle(\|\varphi_1\rangle)$	$\pi/4$	$\pi/4$
$\|\psi_2\rangle(\|\xi_2\rangle)$	$\pi/2$	0	$\|\phi_2\rangle(\|\varphi_2\rangle)$	$-\pi/4$	$\pi/4$
$\|\psi_3\rangle(\|\xi_3\rangle)$	0	$\pi/2$	$\|\phi_3\rangle(\|\varphi_3\rangle)$	$\pi/4$	$-\pi/4$
$\|\psi_4\rangle(\|\xi_4\rangle)$	$\pi/2$	$\pi/2$	$\|\phi_4\rangle(\|\varphi_4\rangle)$	$-\pi/4$	$-\pi/4$

where $\hat{U}_S(\alpha_2)$ can be expressed as

$$\hat{U}_S(\alpha_2) = \begin{pmatrix} \cos\alpha_2 & \sin\alpha_2 \\ \sin\alpha_2 & -\cos\alpha_2 \end{pmatrix}. \tag{7}$$

If we fix $\alpha_1, \alpha_2 \in \{0, \pi/2\}$ or $\alpha_1, \alpha_2 \in \{\pi/4, -\pi/4\}$ and $q = 1/2$, two sets of MUBs, $\{|\psi_i\rangle\}$ and $\{|\phi_i\rangle\}$, are constructed, as shown in Table I. Another two sets of MUBs, $\{|\xi_i\rangle\}$ and $\{|\varphi_i\rangle\}$, can also be constructed in the same way by fixing $q = 1$. These four groups of MUBs can be expressed as

$$\begin{aligned}
&\{|\psi_1\rangle = |H\rangle(|1\rangle + |-1\rangle), |\psi_2\rangle = |H\rangle(|1\rangle - |-1\rangle),\\
&\ |\psi_3\rangle = |V\rangle(|1\rangle - |-1\rangle), |\psi_4\rangle = |V\rangle(|1\rangle + |-1\rangle)\},\\
&\{|\phi_1\rangle = |D\rangle(|1\rangle + i|-1\rangle), |\phi_2\rangle = |D\rangle(|1\rangle - i|-1\rangle),\\
&\ |\phi_3\rangle = |A\rangle(|1\rangle - i|-1\rangle), |\phi_4\rangle = |A\rangle(|1\rangle + i|-1\rangle)\},
\end{aligned} \tag{8}$$

$$\begin{aligned}
&\{|\xi_1\rangle = |H\rangle(|2\rangle + |-2\rangle), |\xi_2\rangle = |H\rangle(|2\rangle - |-2\rangle),\\
&\ |\xi_3\rangle = |V\rangle(|2\rangle - |-2\rangle), |\xi_4\rangle = |V\rangle(|2\rangle + |-2\rangle)\},\\
&\{|\varphi_1\rangle = |D\rangle(|2\rangle + i|-2\rangle), |\varphi_2\rangle = |D\rangle(|2\rangle - i|-2\rangle),\\
&\ |\varphi_3\rangle = |A\rangle(|2\rangle - i|-2\rangle), |\varphi_4\rangle = |A\rangle(|2\rangle + i|-2\rangle)\}.
\end{aligned} \tag{9}$$

III. EXPERIMENT AND RESULTS

The experimental setup is shown in Fig. 3. A continuous-wave laser (1550 nm) is modulated into pulses by an intensity modulator (Oclaro 10 Gb/s modulator, with extinction ratio of 29.2 dB). A variable optical attenuator attenuates the beam into a coherent state with a low photon number. The average photon number is about 0.1 per pulse, which is evaluated at the input of the transmission line, approximating a single photon state. A single-mode fiber filters high-order modes out. The beam, after being aligned into free space by a fiber collimator, is projected on a polarizer to ensure its horizontal polarization. The q plate converts the horizontally polarized photons into vector mode. The half-wave plates (HWPs) and the polarization beam splitter (PBS) together map photons into modes on the equator of the high-order Poincaré sphere, as shown in Fig. 2. The RCF supports vector mode transmission. Two polarization controllers compensate mode crosstalk. A set of half-wave plates and a quarter-wave plate (combined

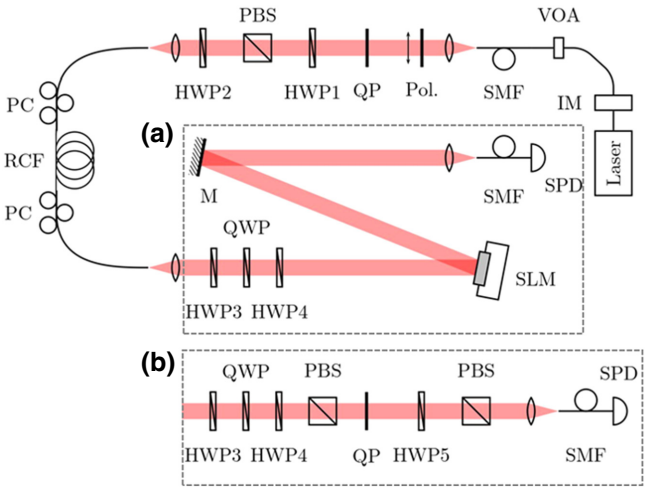

FIG. 3. Experimental setup of high-order quantum cryptography in a RCF. (a) Measurement setup using a SLM for 4 km fiber transmission. Laser wavelength 1550 nm. (b) Measurement setup using a q plate for 4 and 25 km fiber transmission. IM, intensity modulator; M, mirror; PC, polarization controller; Pol., polarizer; QP, q plate; QWP, quarter-wave plate; SMF, single-mode fiber; SPD, single-photon detector; VOA, variable optical attenuator.

with a SLM project the incoming photons into different measurements. The mirror aligns the beam and helps it be coupled into the single-mode fiber, which leads to a single-photon detector (Eos4 from Single Quantum).

We use a 4-km RCF to our high-dimensional quantum-state-distribution system for its easy access and good performance at the lower topological charge of OAM. It is specially designed for transmission of $|\ell| = 1, 2, 3$ OAM modes at 1550 nm. The refractive-index profile of the fiber is shown in Fig. 4(a). The refractive-index difference between the ring core and the cladding is $\Delta n = (n_2 - n_1)/n_1 = 0.7786\%$, in which n_1 and n_2 are the refractive index of the cladding and the ring core, respectively. Figure 4(b) plots the effective refractive index of different eigenmodes in this fiber, while the insets show the simulated intensity profiles of these modes. We also test 25 km of RCF with the same design as a comparison. The simulated and measured (captured by a CCD camera) intensity distributions of modes after 4 km of fiber transmission are shown in Figs. 5 and 6, respectively.

The linear polarization operator $\hat{P}_S(\alpha)$ can be factored into $\hat{P}_S(0)\hat{U}_S(\alpha_1)$. HWP1 functions as the operator $\hat{U}_S(\alpha_1)$, and the PBS functions as $\hat{P}_S(0)$. The product order of these two factors corresponds to the sequence of devices exactly in the real world. Similarly, HWP2 works as $\hat{U}_S(\alpha_2)$. Table I lists the states with several projection angles α_1, α_2. According to Eq. (6), rotating HWP1 changes the projective angle α_1, generating orthogonal OAM superposition states, and rotating HWP2 leads to orthogonal SAM superposition or polarization states. At the output end of the

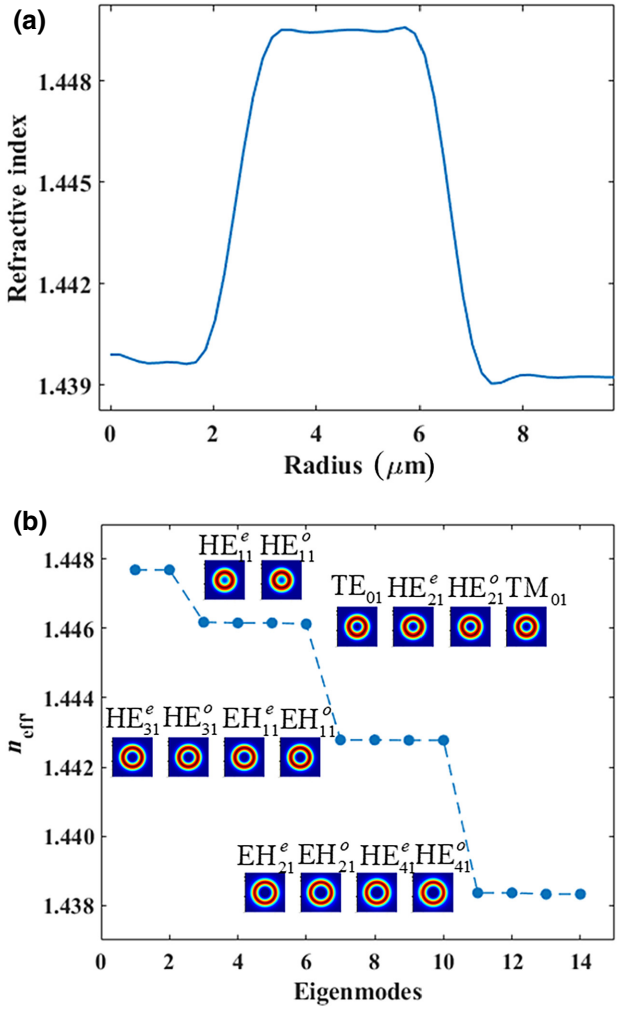

FIG. 4. Fiber information. (a) RCF refractive index versus radius. (b) Simulated OAM eigenmodes of the fiber and effective refractive index.

fiber, HWP3 and the quarter-wave plate together compensate the polarization distortion. The SLM is a tunable polarized phase-control device, so it can be seen as a combination of a PBS, a HWP, and a q plate, which is the main difference between Figs. 3(a) and 3(b). Because of the tunable feature, the SLM is convenient for switching between diverse modes and performing fine adjustment to align the beam by programming. As a comparison, the q plate is a fixed optical component, but it has the potential to be used in the high-speed QKD system for its ability of spin-orbit coupling [16]. Without loss of generality, we test the outcome states on both platforms. For the measurement setup based on the SLM, all projective measurements can be performed with use of HWP4. For the measurement setup using the q plate, rotating HWP4 and HWP5, all states can be measured simultaneously.

According to the Gottesman-Lo-Lütkenhaus-Preskill formula [4], the secret-key rate can be given by $R_d(Q) = \log_2 d - 2h(Q)$ for a single-photon source with 100% error-correction efficiency, where Q is the QBER. By generalizing this formula to higher dimensions, we have $h(Q) = -(1-Q)\log_2(1-Q) - Q\log_2(Q/d-1)$, where d is the dimensionality of the encoding state space. Derived from the Gottesman-Lo-Lütkenhaus-Preskill formula, a secure key can be generated only when the QBER is under a particular threshold value. For two-dimensional subspaces, the threshold is $Q_0^{\rm 2D} = 11.0\%$, while it is $Q_0^{\rm 4D} = 18.9\%$ for four-dimensional subspaces. This gives intuitive insight that high-dimensional quantum cryptography has a higher tolerance to channel loss.

We perform a four-dimensional BB84 protocol through 4 km of RCF. The probability-of-detection matrices are shown in Fig. 7. The corresponding QBERs are $Q_{\ell=|1|} = 4.3\%$ and $Q_{\ell=|2|} = 6.5\%$, respectively. These results are from the measurement setup based on the SLM. For the measurement setup based on the q plate with $q = 0.5$ and $q = 1$ we obtain $Q = 9.4\%$ for $q = 0.5$ with 4 km of fiber, $Q = 12.5\%$ for $q = 1$ with 4 km of fiber, and $Q = 16.3\%$ for $q = 1$ with 25 km of fiber, whose probability-of-detection matrices are shown in Fig. 8. All of them are lower than the threshold value $Q_0^{\rm 4D}$. Table II gives the derived secret-key rates.

IV. DISCUSSION AND CONCLUSION

There are a few practical issues that deserve a mention. In our experiments, we use a weak coherent source, whose photon statistics are engineered to follow a Poisson distribution with a well-defined probability for the emission of a single photon, which is a practical and inexpensive way to probabilistically create single-photon pulses. Although such a source cannot be used to ensure unconditional security against photon-number-splitting attacks, in real-world deployments these attacks could be mitigated through the preparation and transmission of decoy states [38]. As an

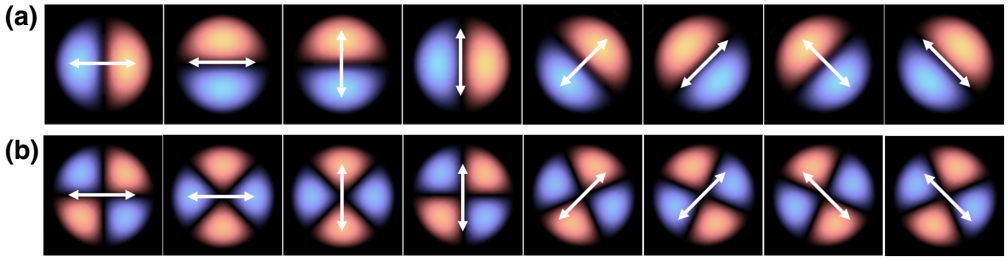

FIG. 5. Mode fields of MUBs. (a) MUBs prepared by a q plate with $q = 1/2$. (b) MUBs prepared by a q plate with $q = 1$. The arrows represent the polarization orientation.

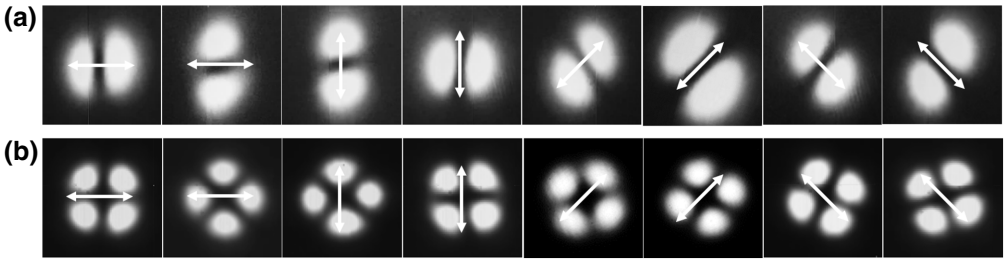

FIG. 6. Measured intensity distributions of modes after the fiber. (a) MUBs prepared by a q plate with $q = 1/2$. (b) MUBs prepared by a q plate with $q = 1$.

alternative, ideal single-photon emitters or heralded photons can be used as the source, requiring no change to the proof-of-principle demonstration outlined here. Furthermore, according to the experimental results, states generated with an $\ell = |1|$ pattern achieve the best conservation performance and the lowest QBER. As longer fiber typically introduces more mode crosstalk and higher ℓ values suffer more channel loss in this fiber, these results conform to our current knowledge. The q-plate measurement for $\ell = |2|$ through 4 km of fiber results in a higher QBER in comparison with SLM measurement. This is due to slight misalignment in free-space coupling and fiber coupling. The higher the QBER is, the more postprocessing required, such as error correction and privacy amplification, leading to lower key rates, until the threshold is exceeded where the channel is considered as unsecured. In our proof-of-concept experiment, the QBERs of different transmitted states are measured one by one by our rotating the HWPs and switching patterns on the SLM manually.

In this proof-of-concept experiment, we realize a four-dimensional quantum-cryptography scheme. These specially designed RCFs with 14 eigenmodes support OAM state transmission up to $\ell = |3|$. All the states in the same MUB set are composed of OAM modes from the same mode group (i.e., $\ell = |1|$ in the second mode group and $\ell = |2|$ in the third mode group). Thus, higher OAM orders should have the same transmission behavior in fibers with a similar design, theoretically. For

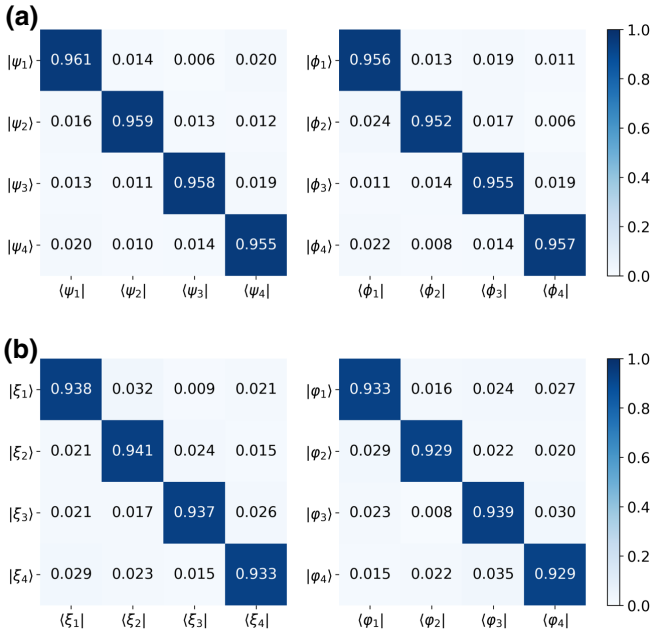

FIG. 7. Experimental probability-of-detection matrices. (a) Annotated heat map of the probability-of-detection matrix for $\ell = |1|$ with measured QBER of $Q = 4.3\%$. (b) Annotated heat map of the probability-of-detection matrix for $\ell = |2|$ with measured QBER of $Q = 6.5\%$.

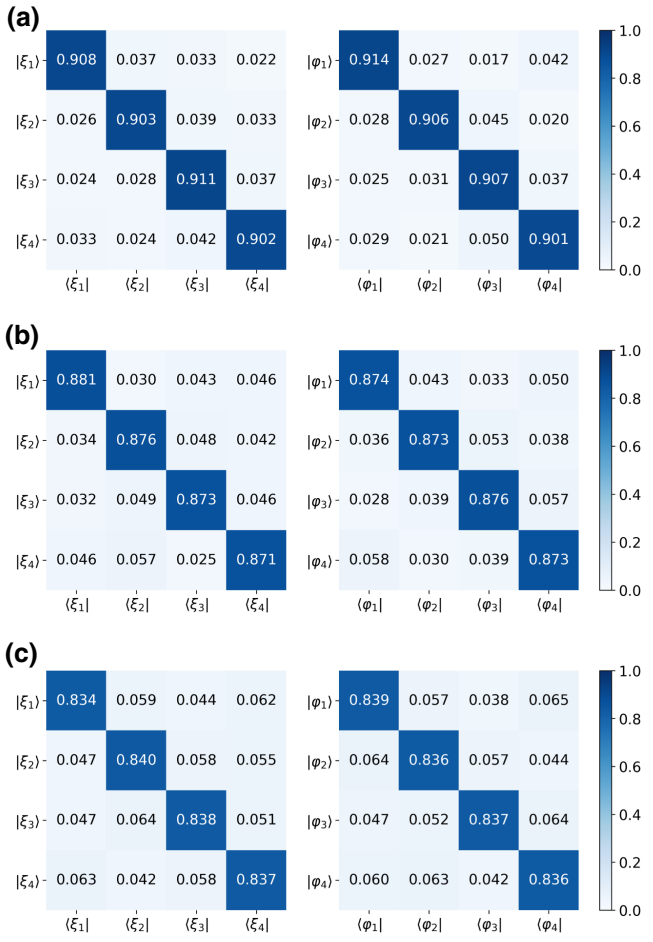

FIG. 8. Experimental probability-of-detection matrices from the q-plate setup for (a) $\ell = |1|$ with 4 km of RCF, (b) $\ell = |2|$ with a 4 km of , and (c) $\ell = |2|$ with 25 km of RCF.

TABLE II. Measured QBERs and secret-key rates for $\ell = |1|$ and $\ell = |2|$.

	SLM measurement		q-plate measurement		
	$\ell = \|1\|$ 4 km	$\ell = \|2\|$ 4 km	$\ell = \|1\|$ 4 km	$\ell = \|2\|$ 4 km	$\ell = \|2\|$ 25 km
QBER (%)	4.3	6.5	9.4	12.5	16.3
$R(Q)$	1.347	1.098	0.807	0.515	0.201

an even-higher-dimensional scheme that includes eigenmodes in a different mode group, mode dispersion will be a big problem. Because of this, we need to find a way to compensate the mode dispersion, such as by using an OAM-mode sorter with another equal-length OAM fiber to compensate the time delay or by optimizing the fiber design so that higher-dimensional QKD systems can be used [16]. Besides, use of an OAM-mode sorter to realize an actively-stabilizing phase precompensation eliminates the intermodal dispersion and makes it feasible to transport high-dimensional OAM entangled photons through a few-mode fiber [30]. Other than its transmission characteristics, some environmental factors, such as temperature fluctuation and mechanical vibration, that act on the fiber tremendously influence the phase stability. The former factor causes a gradual phase drift, while the latter one changes the coupling condition dramatically. To develop a long-distance real-time distribution system, technologies that eliminate phase drift are necessary. A feasible solution is to deploy a phase-correction program by performing phase evaluation after a certain time interval, and then sending adjustment signals to the fiber polarization controller to compensate for phase drift by squeezing the fiber with a piezoelectric ceramic.

The q plate with specific liquid-crystal alignment can be used to realize spin-orbit coupling via geometric phase control. From another perspective, it reveals the nonseparability between OAM and SAM of vector modes, which is indeed the OAM superposition state. By taking advantage of this, OAM-superposition-state manipulation is mapped into polarization manipulation, which is quite mature, leading to a relatively lower QBER [14]. The mapping procedures involve no interferometric structure, significantly reducing the alignment difficulty but increasing stability. In the measurement process, the q plate simplifies the setup and operation as only polarization manipulation is needed.

A SLM is another commonly used projection device. It is a good option for proof-of-concept experiments [39, 40] on account of the high flexibility of phase control. Although it has a limitation of the refresh rate, directly confining the state generation speed [7], we can still take full advantage of its flexibility and generate various phase planes without switching any optical component, while not affecting the validity of the actual scheme. We test the QBER of the setup based on q-plate measurement for a 4-km fiber and a similarly designed 25-km fiber (see Table II). The transmission performance is evaluated for $\ell = |1|$ and $\ell = |2|$ in the same fiber by SLM measurement as well as q-plate measurement. From comparison of the results we obtain, it can be found that QBER of $\ell = |1|$ is lower than the QBER of $\ell = |2|$ for both setups. A QBER less than 10% with the q-plate-measurement setup is also achievable. The QBER for $\ell = |2|$ in the 4-km fiber using q-plate measurement has better performance than in the 25-km fiber. Replacing the SLM-based projection scheme with an OAM-mode sorter and a multichannel q-plate-based scheme results in a high-speed measurement system [16]. Another solution mentioned in Ref. [19], by replacing HWPs with free-space electrical optical modulators, is not practical yet and needs further development.

In conclusion, we generate two sets of MUBs based on SAM-OAM hybrid states by harnessing the merit of spin-orbit coupling and realize the secure transmission of four-dimensional MUBs over a 25-km RCF. The system achieves a relatively lower QBER by using the nonseparable feature of SAM-OAM hybrid states and the transmission characteristics of the RCF. In the scenario of intracity confidential communication, high-dimensional quantum fiber networks guarantee superior security, relatively higher bandwidth, and better noise tolerance. Our work paves the way for improving the performance of high-dimensional quantum-state distribution with SAM-OAM hybrid states. Future investigations should include high-speed real-time quantum-state-distribution realization and fiber design that supports higher-order SAM-OAM hybrid states with more-robust transmission characteristics.

ACKNOWLEDGMENTS

This work was supported by the Key R&D Program of Guangdong Province (2018B030325002), the National Natural Science Foundation of China (Grants No. 11774116, No. 61675189, No. 61905235, and No. 62001182), the Key R&D Program of Hubei Province (Grant No. 2020BAB001), the Science and Technology Innovation Commission of Shenzhen (Grant No. JCYJ20200109114018750), the Open Fund of IPOC (BUPT) (Grant No. IPOC2018A002), the open program from the State Key Laboratory of Advanced Optical Communication Systems and Networks (Grant No. 2020GZKF009), and the Fundamental Research Funds for the Central Universities (Grant No. 2019kfyRCPY037). F.X. Wang and J. Liu were supported by the China Postdoctoral Science Foundation (Grants No. 2019M652179 and No. 2020M672334, respectively).

[1] C. H. Bennett, F. Bessette, G. Brassard, L. Salvail, and J. Smolin, Experimental quantum cryptography, J. Cryptol. **5,** 3 (1992).

[2] V. Scarani, H. Bechmann-Pasquinucci, N. J. Cerf, M. Dušek, N. Lütkenhaus, and M. Peev, The security of practical quantum key distribution, Rev. Mod. Phys. **81**, 1301 (2009).

[3] M. Erhard, R. Fickler, M. Krenn, and A. Zeilinger, Twisted photons: New quantum perspectives in high dimensions, Light: Sci. Appl. **7**, 17146 (2017).

[4] N. J. Cerf, M. Bourennane, A. Karlsson, and N. Gisin, Security of Quantum key Distribution Using *d*-Level Systems, Phys. Rev. Lett. **88**, 127902 (2002).

[5] F. Bouchard, K. Heshami, D. England, R. Fickler, R. W. Boyd, B.-G. Englert, L. L. Sánchez-Soto, and E. Karimi, Experimental investigation of high-dimensional quantum key distribution protocols with twisted photons, Quantum **2**, 111 (2018).

[6] M. Mafu, A. Dudley, S. Goyal, D. Giovannini, M. McLaren, M. J. Padgett, T. Konrad, F. Petruccione, N. Lütkenhaus, and A. Forbes, Higher-dimensional orbital-angular-momentum-based quantum key distribution with mutually unbiased bases, Phys. Rev. A **88**, 032305 (2013).

[7] M. Mirhosseini, O. S. Magaña-Loaiza, M. N. O'Sullivan, B. Rodenburg, M. Malik, M. P. J. Lavery, M. J. Padgett, D. J. Gauthier, and R. W. Boyd, High-dimensional quantum cryptography with twisted light, New J. Phys. **17**, 033033 (2015).

[8] R. Fickler, G. Campbell, B. Buchler, P. K. Lam, and A. Zeilinger, Quantum entanglement of angular momentum states with quantum numbers up to 10, 010, Proc. Natl. Acad. Sci. U.S.A **113**, 13642 (2016).

[9] A. Forbes, M. d. Oliveira, and M. R. Dennis, Structured light, Nat. Photonics **15**, 253 (2021).

[10] A. Forbes and I. Nape, Quantum mechanics with patterns of light: Progress in high dimensional and multidimensional entanglement with structured light, AVS Quantum Sci. **1**, 011701 (2019).

[11] I. Nape, B. Ndagano, B. Perez-Garcia, S. Scholes, R. I. Hernandez-Aranda, T. Konrad, and A. Forbes, High-bit-rate quantum key distribution with entangled internal degrees of freedom of photons, arXiv: Quantum Physics (2016).

[12] A. Sit, F. Bouchard, R. Fickler, J. Gagnon-Bischoff, H. Larocque, K. Heshami, D. Elser, C. Peuntinger, K. Günthner, B. Heim, C. Marquardt, G. Leuchs, R. W. Boyd, and E. Karimi, High-dimensional intracity quantum cryptography with structured photons, Optica **4**, 1006 (2017).

[13] B. Ndagano, I. Nape, B. Perez-Garcia, S. Scholes, R. I. Hernandez-Aranda, T. Konrad, M. P. J. Lavery, and A. Forbes, A deterministic detector for vector vortex states, Sci. Rep. **7**, 13882 (2017).

[14] F. Bouchard, A. Sit, F. Hufnagel, A. Abbas, Y. Zhang, K. Heshami, R. Fickler, C. Marquardt, G. Leuchs, R. w. Boyd, and E. Karimi, Quantum cryptography with twisted photons through an outdoor underwater channel, Opt. Express **26**, 22563 (2018).

[15] A. Sit, R. Fickler, F. Alsaiari, F. Bouchard, H. Larocque, P. Gregg, L. Yan, R. W. Boyd, S. Ramachandran, and E. Karimi, Quantum cryptography with structured photons through a vortex fiber, Opt. Lett. **43**, 4108 (2018).

[16] D. Cozzolino, D. Bacco, B. Da Lio, K. Ingerslev, Y. Ding, K. Dalgaard, P. Kristensen, M. Galili, K. Rottwitt, S. Ramachandran, and L. K. Oxenløwe, Orbital Angular Momentum States Enabling Fiber-Based High-Dimensional Quantum Communication, Phys. Rev. Appl. **11**, 064058 (2019).

[17] M. McLaren, T. Konrad, and A. Forbes, Measuring the nonseparability of vector vortex beams, Phys. Rev. A **92**, 023833 (2015).

[18] J. Liu, I. Nape, Q. Wang, A. Vallés, J. Wang, and A. Forbes, Multidimensional entanglement transport through single-mode fiber, Sci. Adv. **6**, eaay0837 (2020).

[19] F.-X. Wang, W. Chen, Z.-Q. Yin, S. Wang, G.-C. Guo, and Z.-F. Han, Characterizing High-Quality High-Dimensional Quantum key Distribution by State Mapping between Different Degrees of Freedom, Phys. Rev. Appl. **11**, 024070 (2019).

[20] S. Ramachandran, P. Kristensen, and M. F. Yan, Generation and propagation of radially polarized beams in optical fibers, Opt. Lett. **34**, 2525 (2009).

[21] Y. Yue, Y. Yan, N. Ahmed, J. Yang, L. Zhang, Y. Ren, H. Huang, K. M. Birnbaum, B. I. Erkmen, S. Dolinar, M. Tur, and A. E. Willner, Mode properties and propagation effects of optical orbital angular momentum (oam) modes in a ring fiber, IEEE Photonics J. **4**, 535 (2012).

[22] C. Brunet, P. Vaity, Y. Messaddeq, S. LaRochelle, and L. A. Rusch, Design, fabrication and validation of an oam fiber supporting 36 states, Opt. Express **22**, 26117 (2014).

[23] L. Zhu, G. Zhu, A. Wang, L. Wang, J. Ai, S. Chen, C. Du, J. Liu, S. Yu, and J. Wang, 18 km low-crosstalk oam + wdm transmission with 224 individual channels enabled by a ring-core fiber with large high-order mode group separation, Opt. Express **43**, 1890 (2018).

[24] S. Chen, S. Li, L. Fang, A. Wang, and J. Wang, Oam mode multiplexing in weakly guiding ring-core fiber with simplified mimo-dsp, Opt. Express **27**, 38049 (2019).

[25] W. Tian, H. Zhang, X. Zhang, L. Xi, W. Zhang, and X. Tang, A circular photonic crystal fiber supporting 26 oam modes, Opt. Fiber Technol. **30**, 184 (2016).

[26] B. Ung, P. Vaity, L. Wang, Y. Messaddeq, L. A. Rusch, and S. LaRochelle, Few-mode fiber with inverse-parabolic graded-index profile for transmission of oam-carrying modes, Opt. Express **22**, 18044 (2014).

[27] S. Li and J. Wang, Supermode fiber for orbital angular momentum (OAM) transmission, Opt. Express **23**, 18736 (2015).

[28] P. Gregg, P. Kristensen, and S. Ramachandran, Conservation of orbital angular momentum in air-core optical fibers, Optica **2**, 267 (2015).

[29] D. Cozzolino, E. Polino, M. Valeri, G. Carvacho, D. Bacco, N. Spagnolo, L. K. K. Oxenløwe, and F. Sciarrino, Air-core fiber distribution of hybrid vector vortex-polarization entangled states, Adv. Photonics **1**, 1 (2019).

[30] H. Cao, S.-C. Gao, C. Zhang, J. Wang, D.-Y. He, B.-H. Liu, Z.-W. Zhou, Y.-J. Chen, Z.-H. Li, S.-Y. Yu, J. Romero, Y.-F. Huang, C.-F. Li, and G.-C. Guo, Distribution of high-dimensional orbital angular momentum entanglement over a 1 km few-mode fiber, Optica **7**, 232 (2020).

[31] D. G. Hall, Vector-beam solutions of maxwell's wave equation, Opt. Lett. **21**, 9 (1996).

[32] G. Milione, S. Evans, D. A. Nolan, and R. R. Alfano, Higher Order Pancharatnam-Berry Phase and the Angular Momentum of Light, Phys. Rev. Lett. **108**, 190401 (2012).

[33] T. Stav, A. Faerman, E. Maguid, D. Oren, V. Kleiner, E. Hasman, and M. Segev, Quantum entanglement of the spin and orbital angular momentum of photons using metamaterials, Science **361**, 1101 (2018).

[34] E. J. Galvez, S. Khadka, W. H. Schubert, and S. Nomoto, Poincaré-beam patterns produced by nonseparable superpositions of laguerre–gauss and polarization modes of light, Appl. Opt. **51**, 2925 (2012).

[35] F. Cardano, E. Karimi, S. Slussarenko, L. Marrucci, C. de Lisio, and E. Santamato, Polarization pattern of vector vortex beams generated by q-plates with different topological charges, Appl. Opt. **51**, C1 (2012).

[36] L. Marrucci, C. Manzo, and D. Paparo, Optical Spin-To-Orbital Angular Momentum Conversion in Inhomogeneous Anisotropic Media, Phys. Rev. Lett. **96**, 163905 (2006).

[37] A. Rubano, F. Cardano, B. Piccirillo, and L. Marrucci, *Q*-plate technology: A progress review [invited], J. Opt. Soc. Am. B **36**, D70 (2019).

[38] X. Ma, B. Qi, Y. Zhao, and H.-K. Lo, Practical decoy state for quantum key distribution, Phys. Rev. A **72**, 012326 (2005).

[39] Y. Zhou, M. Mirhosseini, S. Oliver, J. Zhao, S. M. H. Rafsanjani, M. P. J. Lavery, A. E. Willner, and R. W. Boyd, Using all transverse degrees of freedom in quantum communications based on a generic mode sorter, Opt. Express **27**, 10383 (2019).

[40] I. Nape, E. Otte, A. Vallés, C. Rosales-Guzmán, F. Cardano, C. Denz, and A. Forbes, Self-healing high-dimensional quantum key distribution using hybrid spin-orbit bessel states, Opt. Express **26**, 26946 (2018).